 SDHM, vol.9, no.2, pp.181-199, 2013

Structural Effect Evaluation of Ballistic Impact on a Shaft by Crystallography

C. Mapelli[1], **A. Manes**[1,2], **M. Giglio**[1], **D. Mombelli**[1]

Abstract: The definition of a complex operative scenario like ballistic damage, that introduces large strains and failure, is a current challenge in the design of critical mechanical components. Aerospace, automotive and manufacturing industries have recently increased their interest in numerical simulations with the long term aim to make these approaches not only reliable enough to reproduce the experimental results but also to provide a trustworthy and effective tool for design. To achieve this aim, the knowledge and calibration of material behaviour is required. Starting from a previous characterization of the constitutive law and ductile failure criterion of Al 6061-T6 aluminium alloy, the present paper evaluates the effects produced by the impact of a bullet on an Al 6061-T6 helicopter transmission rotor shaft. Particular attention is paid to the crystallographic complex texture modifications in microstructural patterns, generated by the ballistic impact. These modifications have been measured on actual damaged specimen, analyzed and compared with results obtained from numerical simulations with the aim to evaluate the effect on the load caring capability of the impacted specimen.

Keywords: Al 6061-T6 alloy, misorientation, helicopter rotor shaft, ballistic impact.

1 Introduction

Safety and reliability in extreme conditions are one of the main issues addressed by mechanical components, especially in the field of aeronautic, automotive and manufacturing industry. A key subject connected to this purpose is the evaluation and assessment of residual structural integrity for critical components whenever interested by damage. In this scenario, the investigation of the damage caused by ballistic impact is very important especially for military aeronautic products. The present work attempts to pursuit such intent by analysing a specific case-scenario

[1] Politecnico di Milano, Dipartimento di Meccanica, Via La Masa 1, 20156 Milan, Italy.
[2] Corresponding Author. Email: andrea.manes@polimi.it; Tel: 0039 02 23998630

with a combination of experimental tests, numerical simulations and detailed crystallographic analyses: the ballistic impact of a 7.62 X 51 NATO ball (soft core) 9.5 g bullet onto a helicopter tail rotor shaft. This is a likely scenario because the helicopters are often employed for low altitude profile missions in hostile environment. The development of a method to evaluate and understand the mechanical modification of the structure following the ballistic impact (connected with the residual load carrying capability) is a challenging task for the aeronautical design sector. In this scenario it is crucial to evaluate the damage caused by ballistic impact on critical mechanical components like the tail rotor shaft. The projectile impact implies extreme load conditions involving very high strain rates combined with high levels of strain [Gilioli, Manes and Giglio (2010), Manes, Peroni, Scapin and Giglio (2011)]. Such extreme conditions can be also found in civil technological processes like trenching, moulding and other techniques, making these simulations a matter of interest also for commercial companies. One of the main aims of this work is to evaluate the localized straining of the material and to point out its dissipation efficiency, observing the texture variations following the bullet impact by means of SEM-EBSD (Scanning Electron Microscopy-Electron Back Scattered Diffraction). As ballistic impact generates significant and complex modifications in the microstructural patterns, the analysis needs to deal and to account for the different parameters and their relative effects onto the crystallographic texture. For instance, high strain rate and local high temperature conditions, involved in the ballistic process, work together in opposite ways: the first causes strain hardening, while the second factor produces softening. Furthermore, after the impact, the cooling process is responsible of other local modifications of the dislocations arrangement and precipitates. Therefore, the experimental analysis attempts to provide a detailed report of the microstructural modifications by comparing the areas close to the damage to the relatively unaffected ones, distant from the damage. Moreover, the influence of these modifications on the mechanical behaviour and on the eventual fracture propagation has been analyzed. The crystallographic textures and the misorientation featuring the grains play in fact a significant role in the fracture mechanism. Grain boundary character has an important role in the cracking process due to the structural and compositional differences among various boundaries. Several authors tried to describe the crack propagation phenomenon, both for transgranular and intergranular, from a crystallographic point of view [Gertsman and Bruemmer (2001); Barella, Mapelli and Venturini (2004); Krupp, Duber, Christ, Kunkler, Schick and Fritzen (2003)]. In particular the misorientation and the CSL distribution (Coincident Site Lattice) are potentially interesting approach to understand how a microstructural and crystallographic configuration either facilitates or blocks crack propagation. EBSD analysis allows the measurement and quantification the misorientation angle and the reciprocal density of coincident sites (Σ). In different

studies, related in particular to intergranular crack but also to short fatigue crack propagation, low misorientation angles seem to be favourable to crack propagation, especially if associated to a high number of Σ3 coincident sites [Gertsman and Bruemmer (2001); Jawad and Zikry (2009)].

Parallel to this evaluation, a detailed Finite Elements Method analysis is performed to numerically reproduce the macro effect of the bullet impact and to associate the specific load and stress conditions to the different areas. According to the FEM analysis results, the texture survey focuses on the most affected areas featuring the most critical conditions (in terms of strain and failure), namely the edges of the bullet-hole and the tip of the crack nucleating from the impact damage. Finally the effect of the damage localized straining of the material is verified monitoring a real crack propagating from the ballistic damage during an experimental torsional fatigue test. Crack propagation is also simulated by means of numerical models, with the calculation of most important crack parameters Thus the three tools involved: experimental ballistic and fatigue tests, numerical models and crystallographic analyses are able to give a comprehensive overview of the residual structural integrity of a mechanical components after a ballistic impact

2 Experimental procedure

2.1 Ballistic experimental tests

The tested rotor shaft consists of a thin-walled cylindrical 760 mm long tube with an external diameter of 63.5 mm and a thickness of 1.7 mm featured by two welded flanges, designed to hold the component in the test configuration (in terms of offset and impact angle of the projectile). The projectile used for the tests is a soft core 7.62x51 ball. It is a *full metal jacket* bullet, with a brass coating and an alloyed lead core. Experimental tests have been performed in a dedicated shooting range, employing a very precise gun with micrometrical controls in pitch and yaw that allow correct and repetitive placement. In addition to this, the main ballistic parameters, i.e. offset and impact angle of the bullet, are set to match the worst possible ballistic condition, according to the contingent load of the shaft: a torque load. This worst condition, defined as the "critical condition", is characterized by an impact angle of 45° (angle of obliquity) and with the projectile surface tangent to the shaft surface: this condition generates a single hole almost elliptical in shape, with an axis tilted at 45° and a maximum damage extension (as far as a single hole is concerned) (Fig. 1). It is not the purpose of this paper to give a detailed description of the ballistic experimental tests; more details concerning the ballistic tests are reported in [Giudici, Manes and Giglio (2010)] and a brief literature survey about such tests can be found in the following publications [Backmann and Goldsmith (1978); Goldsmith

(1999); Dey, Børvik, Hopperstad, Leinum and Langseth (2004); Gupta and Madhu (1997); Forrestal and Piekutowski (2000); Warren and Poormon (2001); Kezhun and Goldsmith (1996)]. Moreover it is important to mention that this impact condition (tangent with 45° oblique angle) has been used for a wider experimental campaign. Damage shapes obtained by the 28 tests vary greatly, even though the initial impact conditions are nominally identical for almost all of the tests. The damage shape ranges from a Ricochet effect, a lateral rebound due to excessive offset, to double hole damage (passing across single hole damage). The reason of this behavior is due to the complex interaction between the supersonic bullet and the air that slightly modify the impact conditions. In 12 specimens the single hole damage has been obtained and in 4 of these specimens the single hole shows similar damage. The activity described in the following has been carried out on these 4 specimens and specifically the detailed texture investigation has been performed on one of these.

Figure 1: Experimental set up of the ballistic test: the shaft specimen is 45° oriented respect to bullet trajectory

2.2 Finite Element (FE) Analysis of the ballistic experimental tests

Numerical simulations are carried out with the finite element commercial code Abaqus\Explicit version 6.10. Analyses simulate the impact of a NATO 7.62 mm ball bullet into the Al-6061-T6 shaft thus reproducing the experimental tests with the bullet configuration of 45° of angle of obliquity and tangent trajectory.

The shaft model exactly reproduces the real nominal scenario; it has a 293,132 solid elements mesh that has been divided into three main areas with the densest one closest to the impact zone (4 brick elements along the thickness of dimensions 0.5x0.5x0.41 mm) to optimize results as a function of computational time [Colombo and Giglio (2007)]. Constrains reproduce overall the real scenario at the tip of the cylinder (Fig. 2a).

The projectile has been modelled as a deformable body and it is has been divided into two parts: jacket and core. For both parts brick elements have been used; in particular the core is composed of 12,488 elements with an average dimension of 0.27 mm. The jacket has instead 6,929 elements with an average dimension of 0.26 mm. Predefined fields which represent the bullet initial translation and spin velocity have been imposed to all bullet elements, respectively equal to 850 m/s and 78.5 rad/s (Fig. 2b).

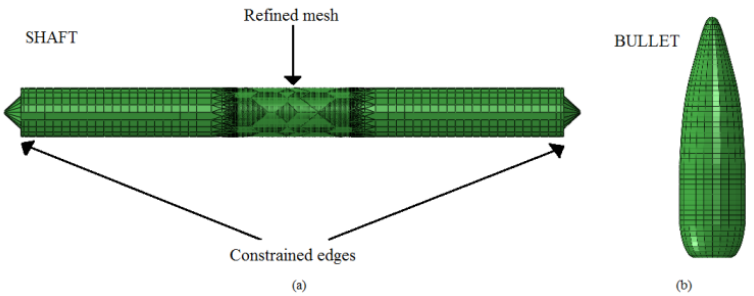

Figure 2: Finite element model of the shaft (a), and of the bullet (b).

As far as the characterization of the material plastic behaviour is concerned, the Johnson-Cook (JC) model has been used for hardening. This model has been widely employed in several ballistic penetration and explosive detonation scenarios providing a reliable constitutive law and a simple calibration in particular for the hardening description where the effect of strain, strain rate and temperature are separated. The JC constitutive law for Al-6061-T6 has been calibrated in previous publications [Gilioli, Manes and Giglio (2010); Manes, Peroni, Scapin and Giglio (2011)]. The adopted fracture criterion is the Bao-Wierzbicki (BW) type [Bao and

Wierzbicki (2004)], previously calibrated for Al-6061-T6 by the authors [Gilioli, Manes and Giglio (2010)]. This phenomenological mode model expresses the trend of strain at failure (ε_f) for the whole field of possible stress triaxiality (η) (where η is often used in damage models and is defined as the ratio between hydrostatic stress and deviatoric stress). This model has been chosen due to the fact that it allows to describe failure onset at different stress triaxiality with good accuracy and has been proved to have a good geometrical transferability property: thus can be calibrated on simple specimens and exploited in more complex cases [Viganò et al. 2012a, 2012b, Manes et al. 2013]. Moreover, a damage evolution phase (after the onset of failure governed by BW criterion) has been introduced: it has been defined in an exponential form through the definition of G_f, the energy needed to open a unit area of crack, evaluated as proposed in [Mabrouki et al. (2008)]. G_f is a function of fracture toughness K_C, Poisson ratio υ and Young modulus E. Using Equation 1, it is then possible to evaluate G_f in the case of more cautionary plane strain case, as suggested in Mabrouki et a. (2008).

$$G_f = \frac{K_{IC}^2}{E}(1-\upsilon^2) \tag{1}$$

Using the mechanical parameters of Al-6061-T6 from NASGRO 4.11 (2004), it is obtained a value of $G_f$equal to 11.2 J/mm^2.

The bullet materials have been modelled using much simpler constitutive laws and fracture criterions [Lumassi, Magrassi, Manes, Bordegoni, and Giglio (2011)], due to lack of data from both the bibliography and manufactures. In particular, for the material of the jacket (brass with 93% Cu, 7% Zn composition) an elastic-plastic behaviour defined for two points is used, whereas the core one (lead-antimony alloy with 87% Pb, 10% Sb, 3% Cu composition) is defined as elastic, perfectly plastic. A ductile failure criterion with a constant ε_f at different triaxiality has been chosen for materials [Lumassi, Magrassi, Manes, Bordegoni, and Giglio (2011)]. The interaction between the projectile and the shaft has been considered; moreover Element Deletion and Nodal Erosion FE options have been activated. For all the elements enhanced hourglass control and element distortion control have been defined. A reduced integration formulation has been used to reduce computational cost. These numerical models allow simulating the phenomenon with good accuracy in terms of residual velocity: 752 m/s compared with an average experimental velocity of 720 m/s (considering the experimental data obtained from the 4 homogeneous specimens).

Residual stresses (RS) have been measured both before and after the impact on the surface of the shafts tested and then compared with the results obtained from FE models. Measures have been performed using an X-ray diffractometer (voltage

analyser Stresstech Group V.1.01). Pre-impact stresses have been measured on all the shafts before the tests with average and standard deviation equal to σ_I= 98 $\pm$ 39 [MPa] and σ_{II} = -29 $\pm$ 39 [MPa]. As far as damaged shafts are concerned, measures have been carried out along the damaged area on a 45° inclined line, respect to the shaft mayor axis (thus crossing the major dimension of the damaged area, the hole). 5 measurement points have been placed before the hole (entry area, 1,2,3,4,5, Figure 3a) and 5 after it (exit area, 6,7,8,9,10, Figure 3a). The nearest measurement point in either direction is placed at a distance of 3 mm from the edge of the hole, and consecutive points are placed at a 2 mm distance from one another, with the exception of the fifth, which is positioned at 5 mm [Giglio and Manes (2011)], Figure 3a. Closer measurements to the damage area are not possible due to the curvature of the surface (petalling). It is important to state that damaged shafts show great variability on of the damaged shape thus a pinpoint comparison of RS is not straightforward both between the whole set of experimental data (the shape of the damage and the RS differ from shaft to shaft) and between experimental and numerical data. According to the measurement points showed in Figure 3a, RS are reported in figure 3b and 3c only for the 4 shafts (specimens #10, #11, #14, #17) with similar single hole damage. High spread in the data is clearly visible underlining the high complex pattern of RS provoked by ballistic impact (also with very similar damage). However a general trend is appreciable: focusing mainly on the values closer to the damage edge (1 and 6) the entry area (before impact) shows prevalence of the traction zone, on the contrary the exit area (after impact) shows a complex pattern with prevalence of the compressive zone in the area where the data have been acquired. However, as previously reported, the RS values have been experimentally acquired relatively distant to the damage. To compare homogenous data, the same procedure (of data mining along a 45° inclined line, respect to the shaft mayor axis) has been used to obtain RS data from the numerical model, Figure 4. Their trends are also reported in Figure 3 b,c (FE model) .

The numerical mode was aimed to reproduce the damage found in the 4 specimens (with similar damage) and it is possible to appreciate in Figure 3 b,c a fairy good correlation that therefore shows the capability of the model to reproduce the RS in these zones.

It is thus possible to draw further conclusions based mainly on FEM data on the whole entry and exit area.

The image produced by the numerical model, in which maximum and minimum residual stresses (σ_I, σ_{II}) have been plotted shows that the entry zone which lies in close proximity of the damage, is mainly subjected to tensile RS (Fig. 4a and 4b). On the contrary the exit zone is more complex to describe: very close the exit apex of the damage both compressive and tensile RS are present (Fig. 4c,d), whereas the

petalling apexes seem to be surrounded by compressive fields (Fig. 4d).

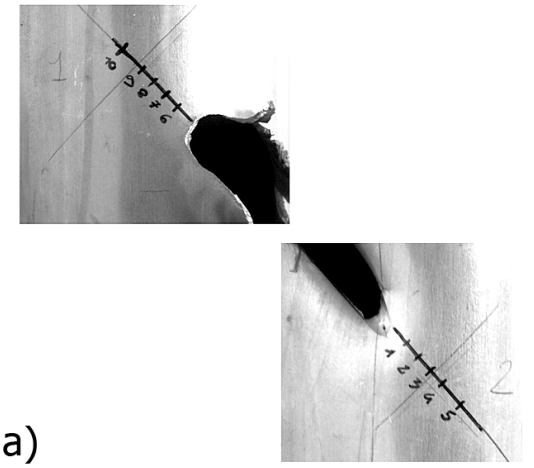

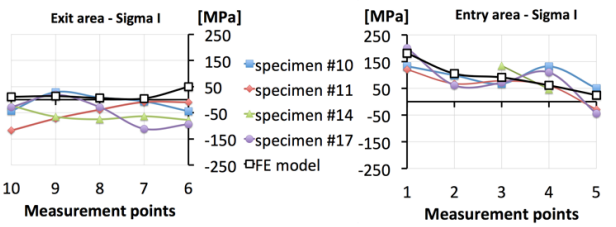

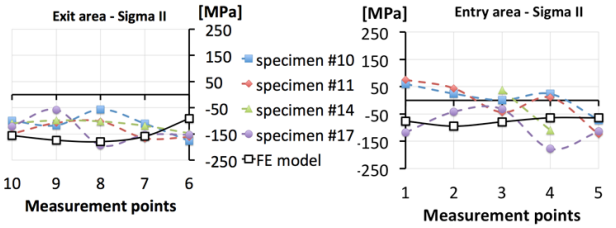

Figure 3: a) Measurement points of residual stresses: 1 to 5 refers to entry area whereas 6 to10 to exit area, b) c) Experimental-numerical comparison of the RS in the entry and exit area.

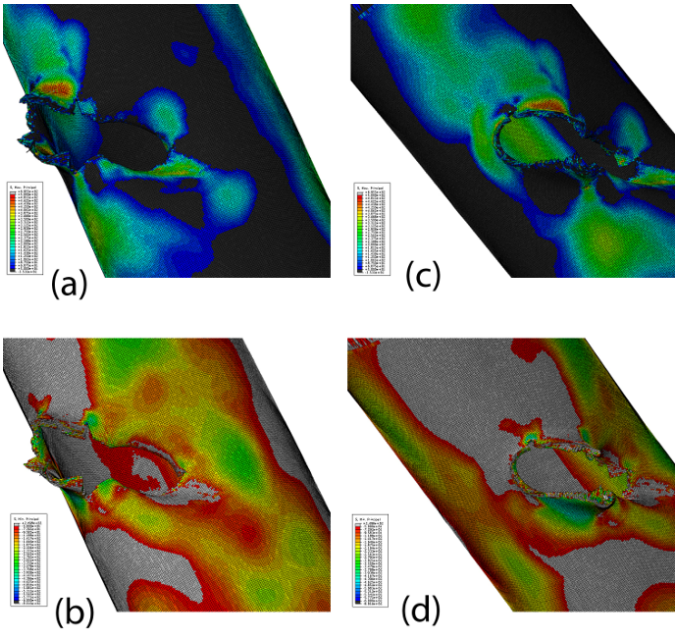

Figure 4: Distribution of principal stresses for inlet (a, σ_I / b, σ_{II}) and outlet (c, σ_I / d, σ_{II}) area of damaged zone obtained from FE simulations.

2.3 Texture investigations in experimental tests

The experimental procedure for crystallographic texture investigations involves mechanical grinding followed by chemical electro-polishing. Following the standard procedure for mechanical grinding, the samples (obtained from one of the four homogeneous specimens before described) are initially polished using an aqueous solution of colloidal SiO_2(0.2 μm) and subsequently electro-polished by Struers Movipol equipment using the following electrolyte solution: 140 ml H_2O, 800 ml C_2H_5OH and 460 ml $HClO_4$ [ASM Metal Handbook (2004)]. This treatment is designed to remove the surface oxide layer to enhance the backscattered signal emitted by the surface, a crucial requirement for the EBSD analysis. The SEM instrumentation employed for the experimental work is a Carl Zeiss AG - EVO®50 Series and the rolling direction (RD) taken during the measurement corresponds to the nominal trajectory of the bullets on the shaft (the 45° impact angle), as reported in Fig. 6. The pixel area of the digital image for the texture corresponds to 7.02 μm^2, the magnification used is 500x. The EBSD picture therefore includes 740x540 pixels and the working distance of the EBSD probe is 16.5 mm and 20 kVx1 nA is applied.

The highlighted areas in Fig. 5 correspond to the rotor shaft damaged part and to the sites where the investigated specimens are harvested. Sample #2 and #6 have been taken in the area adjacent to the exit zone of the projectile; this area is affected mainly by compressive residual stresses, (Fig. 4b and 4d). Sample #3 and #5 have been taken in the area adjacent to the entry zone of the projectile; this area is mainly affected by tensile residual stresses [Gao, Kunnar, Nalla and Ritchie (2005)], (Fig. 4a). Moreover, the work includes an analysis of the cracks originating from the edge of the damage area; namely specimen #1 and #4 refer, respectively, to the crack-tip affected by compressive and tensile stress fields. These cracks (and in particular the crack related to specimen #1) propagated due to a fatigue torsional spectrum applied to the damaged shaft (thus after the ballistic damage). More details about fatigue test are reported in the following section. Specimen 7 has been chosen as an undamaged reference zone (far from the damage).

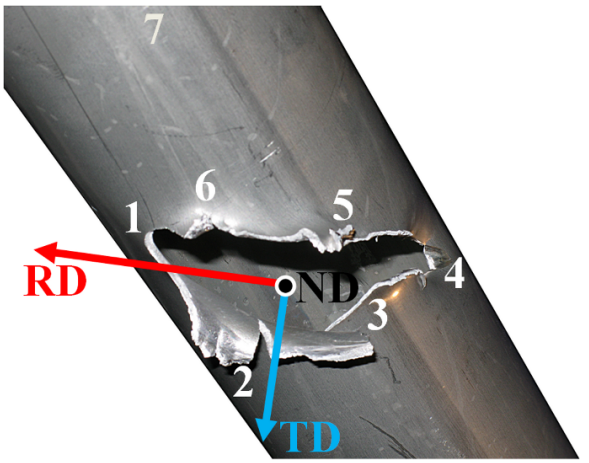

Figure 5: Reference system employed for the EBSD analysis (RD=Rolling Direction, TD=Transverse Direction and ND=Normal Direction) and samples nomenclature.

3 Results

The following section reports the main experimental findings from both Finite Element Analysis and the SEM-EBSD investigations. The critical areas identified in the previous section are analysed herein using the EBSD technique to investigate the texture evolution associated to the high-speed impact of the bullet. Moreover the section attempts to provide a simulation (by means of the numerical model previous presented) of crack propagation inside the stress field provoked by the

ballistic impact comparing the results and behaviour obtained with the texture evolution.

As demonstrated in a previous preliminary study by the same authors [Mapelli, Manes, Giglio, Mombelli, Baldizzone, Gruttadauria(2011)], EBSD analysis is a useful instrument to understand how the crystallographic configuration of materials after damage can promote or inhibit crack propagation. In particular, the analysis performed on the crack flaps shows that the projectile induces a texture pattern that is favourable to crack propagation, because grains misorientations revealed a high number of grain boundary characterized by low angle. In this survey both crack flaps and apex are investigated and the analysis in an area far from the damage is performed to define a reference status.

Fig. 6 shows the SEM pictures of the crack apexes, corresponding to the investigated areas #1 and #4, whereas, Fig.7 shows the diffraction map obtained at the crack apex and the comparisons of the crack apex with the undeformed region.

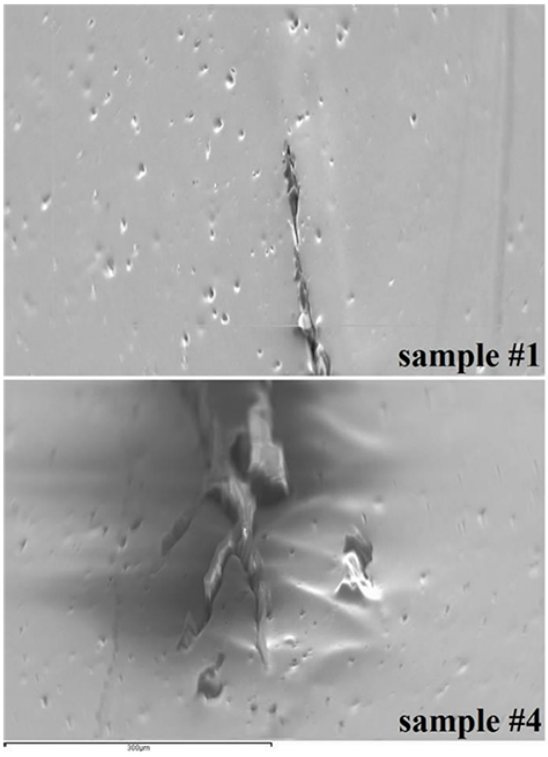

Figure 6: SEM picture of the crack apexes.

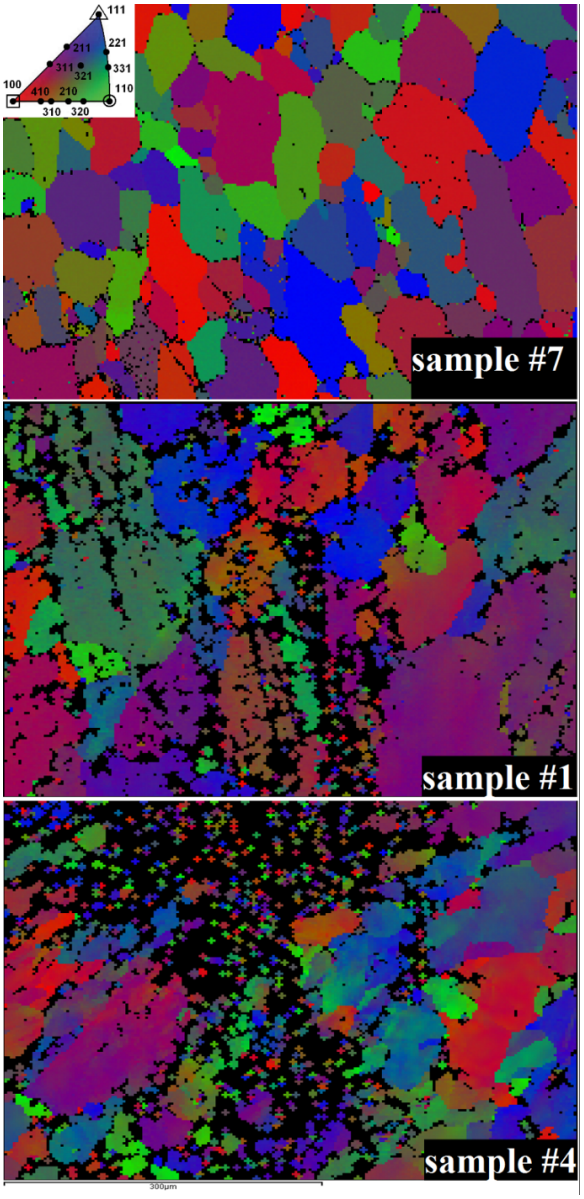

Figure 7: EBSD diffraction map of sample #1 and #4 compared with undeformed reference point (#7) referred to the RD direction.

The high number of unresolved points in the diffraction maps is caused by the non-planarity of the crack surfaces that diffract the backscatter electrons out from the phosphorous screen. The presence of some pits and the deformation in the zone near the damage contribute to a further increase of the number of unresolved points.

The diffraction maps show an alignment of <$\underline{1}$12>, <$\underline{1}$13>, <$\underline{1}$23>, <$\underline{1}$22> and <$\underline{1}$33> lattice directions along the rolling direction, RD, or in another words, along the direction of the ballistic impact and the damage propagation. Moreover, the direction [101] is strongly aligned along ND. Inverse polar figures (Fig. 8) summarize the activated directions along the reference system selected for the analysis.

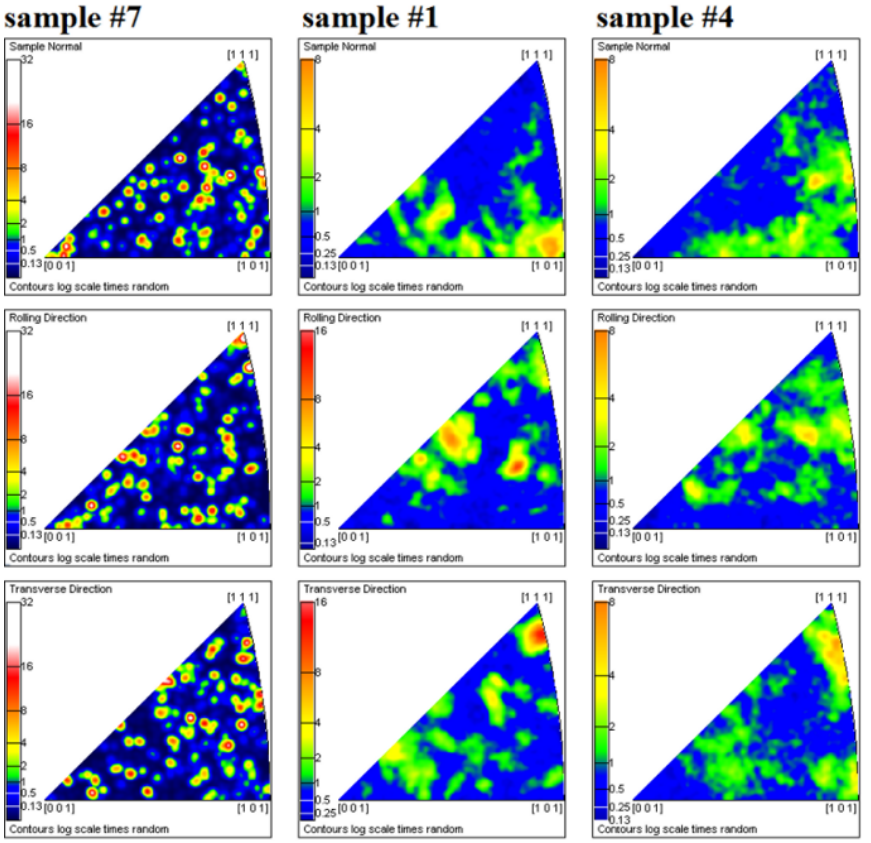

Figure 8: Inverse polar figures related to samples #1,#4 and #7 along ND, RD and TD directions.

The damage seems to cause a transition from an isotropic dispersion (sample #7) to a narrower range of preferential directions aligned along the damage surface.

Strong anisotropy is also shown by the material with respect to the normal direction (ND) that corresponds to the plane in which lips of the petalling of the damage have been ripped.

The recrystallised and highly deformed area is closest to the crack apexes (areas #1 and #4) whereas the material far from the damaged area retains a high number of randomly oriented grains [Mapelli, Manes, Giglio, Mombelli, Baldizzone, Gruttadauria (2011)].

A fatigue torsional spectrum (composed by three load levels) representing the operating loads detected during a recovery mission at reduced power, has been applied on a damaged shaft specimen (one of the four homogeneous specimens before highlighted) by means of a hydraulic multiaxial test machine MTS 809. Monitoring the crack during the torsion-loading test on the damaged shaft [Giglio and Manes (2011)] shows rapid crack propagation during the application of the first load level (the highest one). During the application of this first load level a fatigue crack nucleates at the exit apex (edge #1) of the hole, and propagates from this point. Crack propagations have been monitored by means of a Leica DFC290 optical microscope, equipped with the hardware and the software for image acquisition to measure the position of the crack tip. The propagation of the crack has been numerically simulated (on the damaged model presented in section 2.2) with discrete steps and the SIFs (stress intensity factor) K_I, K_{II} and K_{III} have been acquired at each step. K values are locally calculated by the FE solver (ABAQUS) directly through an internal algorithm and the growth of the crack has been evaluated by an equivalent SIF value (Keq), equation 2, and NASGRO relationship.

$$\Delta K_{eq} = [\Delta K_I^2 + \Delta K_{II}^2 + (1+\upsilon)\Delta K_{III}^2]^{0.5} \tag{2}$$

Keq of equation 2 is based on Strain Energy Release Rate from the work of Irwin, reported in Socie and Marquis (2000). The use of a formulation to combine SIFs values is necessary due to mode III propagation is not negligible (it is likely to be due to the shape and extension of the damage) and have to be considered: during the torsional cycles there is a not planar separation of the crack surface that leads also to a not negligible mode III contribution in the propagation. In particular mode III becomes significant when crack propagation overcame 1.5 mm. The numerical simulation results show that the presence of the RS pattern (obtained from the simulation of the ballistic impact) leads to a not monotone increment with rapid crack propagation especially during the application of first part of the load level 1, Figure 9. The agreement between experimental and numerical propagation is very encouraging Figure 9. It is important to state that the numerical propagation data reported in Figure 9 are obtained from a two-steps numerical modelling approach. The propagation "bed" is in fact the numerical model, obtained simulating

the ballistic impact, on which the propagation stage is subsequently simulated. As explained in the text, the impact phenomena lead to a complex damage shape and multiaxial stress field in the area interested for the crack propagation. The accuracy of the propagation data is therefore also deeply related to the first stage of simulation. Material behaviour, impact condition and numerical issues have to be considered in detail in order to achieve valuable results. With these premises, a numerical approach that is able to replicate the crack propagation phenomena both globally (the crack length after about 2000 cycles is very similar) and the trend (fast propagation of a crack very near to the apex of the damaged area) can be considered a good result. Better results can be obtained improving the first stage: impact. In particular is opinion of the authors that a more refined material characterization of the bullet (both for lead core and bras jacked) would allow to describe better the complex interaction between bullet and shaft during the impact and consequently the shape and the stress field of the damage associated (where crack propagates).

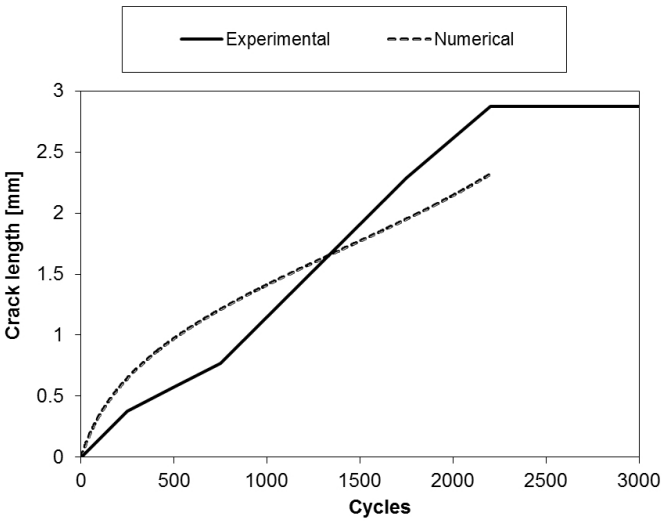

Figure 9: Comparison between experimental and simulated (by means of a numerical model and NASGRO relationship) propagation of a crack nucleated from the ballistic damage under fatigue torsional load.

As far microstructure is concerned for the very first part of crack propagation (specimen #1 was harvested in the edge of the ballistic damage this is representative of the very first part of the crack propagation), the crystallographic configuration induced by the ballistic impact most likely contributes to the rapid progression of the nucleated crack (due to the damage). When the crack reaches the unaltered pattern,

its dimensions have reached a point where the propagation depends only on a mechanical phenomenon, even though the crystallographic configuration can reduce the propagation rate.

The analysis of the CSL boundary and misorientation (Fig. 10) support the hypothesis based on the EBSD results. This hypothesis states that the impact between the material and projectile, due to the high energy provided, is able to transform the microstructure and promote the local recrystallization (high number of Σ3 CSL in the samples #1 and #4).

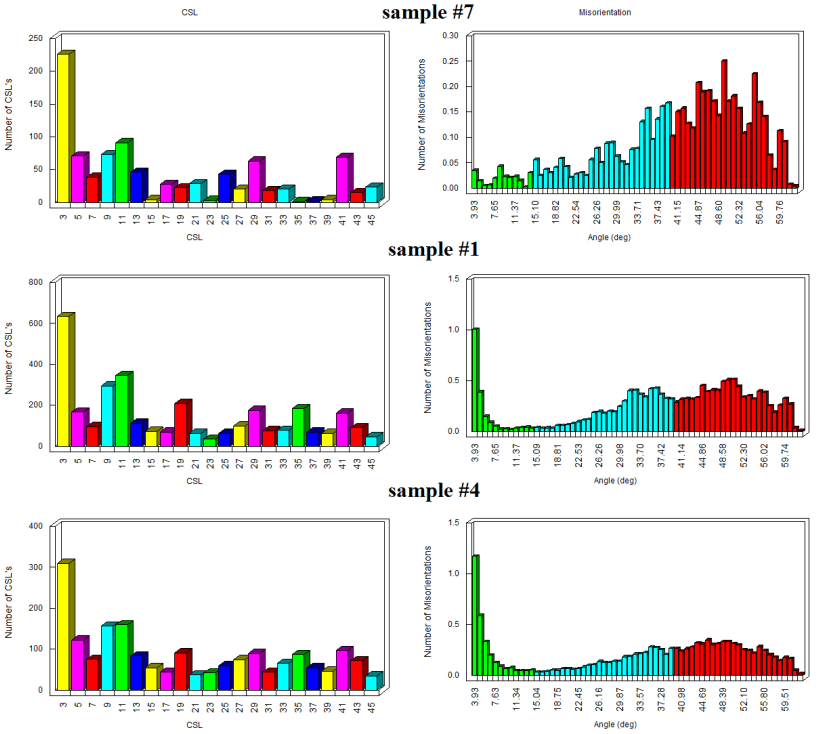

Figure 10: CSL boundary and misorientation relative to undeformed (#7) and crack apexes (#1; #4)

This transformation increases the number of grains at a low angle respect the adjacent, and this increase in number in turn appears to increase the capacity of the material to propagate cracks from the apexes of the damaged area. The main reason for this behaviour is that the fatigue crack does not recognise the grain boundaries featured by low orientation and can, thus, propagate more easily. Because of the crystallographic pattern of near grains is similar to each other, the crack could

propagates on the same crystal system without significant deviations. The grain boundaries are not recognized by the crack due to the low misorientation angles. Thus after the nucleation, the crack can propagate in a situation very similar to single grain material, without meet any obstacle that could arrest or modify the crack propagation direction.

4 Conclusions

The work presented deals with a compound of experimental tests, numerical simulations and crystallographic analyses aimed to a survey on the residual structural integrity of a helicopter rotor shaft subjected to a ballistic impact. The following conclusions can be drawn:

- the damage process due to impact determines a strong orientation of the grains (close to the edges of the ballistic damage) along the direction of the ballistic impact (RD direction);
- the increased orientation distribution of the smaller grains detected on the crack apexes of the damage (sample #1, #4) can be caused by the high strain, the strain rate and the temperature associated to the impact of the bullet, which triggered a recrystallization of the lattice.
- the comparison of the misorientations in the undeformed areas (sample #7) with the areas affected by the ballistic impact and in particular the areas from which cracks have nucleated and eventually propagated (sample #1, #4) yields a decrease in the boundary angle values (lower than the 15° limit). This decrease allows cracks to proceed undisturbed by the grain boundaries.
- experimental tests and the numerical models of the crack propagation from the damaged shaft under torsional loading show the tendency of the material to fast propagation of a crack very near to the apex of the damaged area; however it is important to state that this effect is, in a numerical model, due to residual stress features and shape of the damaged are (petalling) and not directly related to a grain scale simulation.

Thus concluding experimental fatigue tests, numerical models and crystallographic investigation confirm the criticality of such type of ballistic damage in terms of residual structural integrity.

References

ASM Metal Handbook (2004): *Metallography nad Microstructure*, vol. 9, ASM International, Materials Park (OH), USA.

Backmann, M. E.; Goldsmith, W. (1978): The mechanics of penetration of projectiles into targets. *Int. J. Eng. Sci.,* vol. 16, pp. 1–99.

Bao, Y.; Wierzbicki, T. (2004): A comparative study on various ductile crack formation criteria. *J. Eng. Mater. Technol.* – Volume 126, Issue 3 pp. 314-324

Barella, S.; Mapelli, C.; Venturini, R. (2004): Investigation about the stress corrosion cracking of Ti-6Al-4V. *Metallurgical Science and Technology*, vol. 22-2, pp. 19-26.

Colombo, D.; Giglio, M. (2007): Numerical analysis of thin-walled shaft perforation by projectile. *Computers & Structures, Elsevier Applied Science*, vol. 85, pp. 1264-1280.

Dey, S.; Børvik, T.; Hopperstad, O. S.; Leinum, J. R.; Langseth, M. (2004): The effect of target strength on the perforation of steel plates using three different projectiles nose shapes. *Int. J. Impact Eng.,* vol. 30, pp. 1005-1038.

Forrestal, M. J.; Piekutowski, A. J. (2000): Penetration experiments with 6061-T6511 aluminum target and spherical nosed projectiles at striking velocities between 0.5 and 3.0 km/s. *Int. J. Impact Eng.,* vol. 24, pp. 57-67.

Gao, Y.;Kunnar, M.; Nalla, R. K.; Ritchie R.O (2005): High-Cycle Fatigue of Nickel-Based Superalloy ME3 at Ambient and Elevated Temperatures: Role of Grain-Boundary Engineering. *Metall. Mater. Trans.,* vol. 36-12, pp. 3325-3333.

Gertsman, V. Y.; Bruemmer, S. M. (2001): Study of grain character along intergranular stress corrosion crack paths in austenitic alloys. *Acta mater.*, vol. 49, pp. 1589-1598.

Giglio, M.; Manes, A. (2011): Terminal ballistic effect on the crack growth assestement of a helicopter rotor drive. *Eng. Fracture Mechanics*, vol. 78, pp. 1542-1554.

Gilioli, A.; Manes, A.; Giglio, M. (2010): Calibration of a constitutive material model for Al 6061-T6 aluminium alloy. *Proceedings of ACE X2010*, Paris (France).

Giudici, L.; Manes, A.; Giglio, M. (2010): Ballistic Impact on a Tail Rotor Transmission Shaft for Helicopter. *Proc. of Ballistic 2010*, Beijing (China).

Goldsmith, W. (1999): Non-ideal projectile impact on targets. *Int. J. Impact Eng.,* vol.22, pp. 95-395.

Gupta, N. K.; Madhu, V.; (1997): An experimental study of normal and oblique impact of hard-core projectile on single and layered plates. *Int. J. Impact Eng.,* vol. 19, pp. 395-414.

Jawad, F. F.; Zikry, M. A. (2009): The Effects of Grain-boundary Orientations on Failure Behavior in F.C.C. Polycrystalline Systems. *Int. J. of Damage Mechanics*,

vol. 18-4, pp.341-369

Kezhun, L.; Goldsmith, W. (1996): Impact on aluminum plates by tumbling projectiles: experimental study. *Int. J. Impact Eng.,* vol 18, pp. 23-43.

Krupp, U.; Duber, O.; Christ, H. J.; Kunkler, B.; Schick, A.; Fritzen, C. P. (2004): Application of the EBSD technique to describe the initiation and growth behavior of microstructurally short fatigue crack in a duplex steel. *Journal of Microscopy*, vol. 213-3, pp. 313-320.

Lumassi, D.; Magrassi, A.; Manes, A.; Bordegoni, M.; Giglio, M. (2011): Analysis of terminal ballistic into a helicopter drive shaft impacted by NATO 7.62 mm bullet: tests and simulations. *Proceedings of 3rd ICILLS2011*, Valencieennes (France).

Mabrouki, T.; Girardin, F.; Asad, M.; Rigal, F. (2008): Numerical and experimental study of dry cutting for an aeronautic aluminum alloy. *Int. J. of Machine Tools and Manufacture,* vol. 48, pp. 1187-1197.

Manes, A.; Peroni, L.; Scapin, M.; Giglio, M. (2011): Analysis of strain rate behavior of an Al 6061 T6 alloy. *Procedia Engineering,* vol. 10, pp. 3477-3482.

Manes, A.; Gilioli, A.; Sbarufatti, C.; Giglio, M. (2013): Experimental and numerical investigations of low velocity impact on sandwich panels. *Composite Structures*, vol. 99, pp. 8-18.

Mapelli, C.; Manes, A.; Giglio, M.; Mombelli, D.; Baldizzone, C.; Gruttadauria, A. (2011): Crystallographic investigation of ballistic impact of a 7.62 NATO bullet on a Al 6061 T6 transmission shaft. *Procedia Engineering,* vol. 10, pp. 3447-3452.

NASGRO 4.11 (2004): Reference Manual, NASA Johnson Space Center.

Socie D.F. and Marquis G.B. (2000):"Multiaxial Fatigue", SAE.

Viganò, F.; Manes, A.; Giglio, M. (2012a): Numerical simulation of the slant fracture of a helicopter's rotor hub with a ductile damage failure criteria. *Fatigue and Fracture of Engineering Materials and Structures*, vol. 35, issue 4, pp. 317–327.

Viganò, F.; Manes, A.; Giglio, M. (2012b): Ductile fracture locus of Ti-6Al-4V titanium alloy. *International journal of mechanical science,* vol. 54, pp. 121–135

Warren, T. L.; Poormon, K. L. (2001): Penetration of 6061 T6511 aluminum targets by ogive-nosed VAR 4340 steel projectiles at oblique angles: experiments and simulation. *Int. J. Impact Eng.,* vol. 25, pp. 993-1022.